DEVELOPMENTAL BIOLOGY **203,** 245–263 (1998)
ARTICLE NO. DB989016

The Shaping of Pharyngeal Cartilages during Early Development of the Zebrafish[1]

Charles B. Kimmel,[2] Craig T. Miller, Greg Kruze, Bonnie Ullmann, Ruth A. BreMiller, Karen D. Larison, and Hannah C. Snyder

Institute of Neuroscience, 1254 University of Oregon, Eugene, Oregon 97403-1254

In zebrafish the cartilages of the pharynx develop during late embryogenesis and grow extensively in the larva before eventually being replaced by bone. Here we examine chondrocyte arrangements, shapes, numbers, and divisions in the young hyoid cartilages. We observe two distinct developmental phases, morphogenesis and growth. The first phase generates stereotypically oriented chondrocyte stacks that might form by intercalations among cells within the precartilage condensations. In mutants that have deformed cartilages the orientation of the stacks is changed, and we propose that their correct formation underlies the correct initial shaping of the organ. The following period of rapid, nearly isometric cartilage growth occurs by divisions of chondrocytes that are largely located near the joints, and appears to be under quite separate regulation.

INTRODUCTION

During evolution major changes have occurred in the shapes of the body organs of multicellular organisms. Organ shape is an attribute that appears in a complex way during ontogeny, and we have little understanding of how genes control the development of the specific shapes of organs, or even what cells in or around a developing organ do to shape it correctly. A reasonably complete understanding of both development and evolution of organ form would seemingly require such knowledge. Only then will we begin to understand how genotypes translate, through developing cells and their morphogenetic behaviors, into organ morphologies.

The shapes of cartilages and bones are of particular interest because skeletal function, acted upon by natural selection, is directly related to skeletal morphology. In part because bones preserve well as fossils, the skeleton has played the major role in understanding vertebrate evolution; the skeleton of the pharynx particularly has undergone substantial change (review; Kuratani *et al.*, 1997; Forey and Janvier, 1993; Rowe, 1996). The skeleton is relatively simple in cellular terms. In the case of cartilages, neither blood vessels nor marrow nor nerves invade the organ. Rather, a cartilage includes only two cell types: the chondrocyte within the matrix of the organ and the perichondrial cell in its enveloping mesenchyme. This relative simplicity makes cartilage attractive for cellular-level analysis of organ shape. Furthermore, in fishes the chondrocytes have only a thin shell of extracellular cartilage matrix (Beresford, 1993), which allows us to focus on cellular organization in considering how the cartilage is shaped.

In this paper we consider cartilages that develop in the hyoid arch (the second pharyngeal arch) of developing zebrafish. The cartilages in this arch come in a variety of shapes and sizes (Fig. 1A), that serve to support the jaw, buccal cavity, and operculum and the hyoid cartilages can be readily visualized in the living preparation (e.g., Fig. 1B; see also Kimmel *et al.*, 1995). As in other vertebrates, the pharyngeal cartilages arise at least in part from cells that migrate from the region of the cranial neural crest (Schilling and Kimmel, 1994). Migration occurs during the first embryonic day, the beginning of a complex course of morphogenesis. The migrating cells form distinctive condensations of precartilage mesenchyme (reviews: Thorogood, 1983; Hall and Miyake, 1992) within the pharyngeal segments, or branchiomeres, and their chondrification begins during the second embryonic day (Schilling and Kimmel, 1997). In the lateral wall of the hyoid arch two separate sites begin to chondrify nearly simultaneously within a large, apparently

[1] This paper is dedicated to Peter V. Thorogood, who died during August, 1998. Dr. Thorogood carried out pioneering research on cartilage morphogenesis.

[2] To whom correspondence should be addressed. Fax: (541) 346-4548. E-mail: kimmel@uoneuro.uoregon.edu.

0012-1606/98 $25.00

single hyoid condensation (Bertmar, 1959; see also Goodrich, 1930; De Beer, 1937). These sites will develop into the two prominent cartilages that articulate: the dorsolateral hyomandibular (HM) and the ventrolateral ceratohyal (CH). Within an hour or so, a small third site of chondrification appears within the same condensation that will form a symplectic (SY) region of cartilage. During the third (and last) embryonic day, the HM and SY fuse together into a single hyosymplectic (HS), and a third cartilage, the small interhyal (IH), appears in the developing joint between the HS and the CH.

Here we examine the organization and divisions of chondrocytes during the early development of the hyoid cartilages. A key finding is that an early period of morphogenesis in the embryo is followed by a largely separate period of growth in the larva. As we illustrate with the HS, the initial cell arrangements are simple and stereotyped, and correlate with the form of the organ. In particular, the cells develop stacks that lie in parallel with the organ's long axis. During cartilage growth chondrocytes divide within particular regions of the early cartilages in a way that generally preserves the organ shape while largely obliterating the early cell stacks. Mutations are available that disrupt zebrafish cartilage development (Neuhauss *et al.,* 1996; Schilling *et al.,* 1996a; Schilling *et al.,* 1996b; Piotrowski *et al.,* 1996; reviewed in Schilling, 1997), and we compare the hyoid cartilage phenotypes resulting from mutations at three loci. The deformations are highly variable, but can all be fit into a single "phenoytypic series," suggesting that the three genes all act on a single morphogenetic pathway. A change in the orientation of chondrocyte stacks accompanies the change in cartilage shape, supporting the view that control of stack assembly is a critical feature in cartilage organogenesis.

MATERIALS AND METHODS

Animals

Embryos and larvae of the zebrafish *Danio (Brachydanio) rerio* were of the inbred AB strain, obtained from natural spawnings and maintained in embryo medium at 28.5°C as described (Westerfield, 1995). Times refer to hours or days postfertilization; hatching occurs between days 2 and 3 (Kimmel *et al.,* 1995). Preliminary experiments showed a high correlation between the rates of growth of young larvae and their pharyngeal cartilages. Hence for the growth experiments reported below, the larvae were kept uncrowded (at or below 20 individuals/150 ml) and fed with excess paramecia to ensure a high growth rate (an approximately linear increase in body length of 360 μm/day through the period of 4–10 days). Mutant strains (*sucker*^{tf216b}, *schmerle*^{tg203e}, *sturgeon*^{td204e}, Piotrowski *et al.,* 1996) were obtained from the Max Planck-Institut für Entwicklungsbiologie (Tübingen, Germany) and crossed onto the AB background. Heterozygotes were intercrossed to obtain homozygous mutant larvae.

Cartilage Staining and Analysis

Staged embryos and larvae were anesthetized with buffered ethyl-*m*-aminobenzoate methane sulfanate (Westerfield, 1995) and killed by immersion either in 4% formaldehyde (prepared from paraformaldehyde, and buffered to pH 7 in phosphate-buffered saline (PBS)) or in 5% trichloroacetic acid, the latter resulting in poorer preservation but in which unstained cells are more readily visible with Nomarski optics. The fixed animals were rinsed in acid–alcohol (0.37% HCl, 70% EtOH), and stained overnight in either Alcian blue (Schilling *et al.,* 1996a) or Alcian green (0.1% in acid–alcohol). After differentiation in several changes of acid–alcohol the preparations were rehydrated, and the tissue was softened by digestion for 1–5 min with 1.67% trypsin. Following rinsing and clearing in a solution of 50% glycerol and 0.25% KOH, the pharyngeal cartilages were dissected free from surrounding tissues with fine stainless-steel minutien pins, mounted in glycerol or 50% glycerol, 0.25% KOH, and sealed under coverslips. For the preparations described in Figs. 4 and 5, images of the stained and flat-mounted cartilages were digitized, and custom software was used for shape and size analyses. Changes in the thickness of the cartilage plates are ignored in these data.

Other specimens from 2.5 to 8 days old were fixed in Bouin's fixative and embedded in Epon, and serial sections were cut at 3–7.5 μm in one of the standard planes. The sections were stained with methylene blue and basic fuchsin (Humphrey and Pittman, 1974).

Vital Labeling of Chondrocytes

Cells were labeled with the lineage tracer dye rhodamine–dextran (Molecular Probes, 10,000 Da) by intracellular injection during mid- and late blastula stages, resulting in large labeled clones (Kimmel *et al.,* 1994). At 3 days we sorted through embryos to find ones with one or only a few labeled cells in the symplectic (SY), and photographed the cells under epifluorescence using a high-gain silicon intensified video camera. We then took a through-focus series of Nomarski images of the SY with a second camera, this time at high resolution, and from these images reconstructed the stack of unlabeled cells in the SY. The labeled cells, although dim, could also be detected with this camera, such that the assignment of their positions along the stack was unambiguous. The larvae were incubated for another day, and the procedure was repeated at day 4.

Bromodeoxyuridine (BrdU) Labeling

Animals were incubated in 1 mM BrdU in embryo medium and fixed in 4% formaldehyde in PBS. Incorporation of BrdU was detected with anti-BrdU primary antibody (antibody G3G4 developed by S. J. Kaufman and obtained from Developmental Studies Hybridoma Bank, Univ. of Iowa), horseradish peroxidase-conjugated secondary antibody (Sigma), and stained for peroxidase with diaminobenzidine and hydrogen peroxide, as described by Hatta *et al.* (1991) with the following modifications: Following rehydration, larvae were permeabilized with a 10 μg/ml proteinase K solution for 1 h to increase antibody penetration. The preparations were then refixed in 4% formaldehyde for 30 min, rinsed in water, and then treated with 2 N HCl for 1 h to denature DNA. Larvae were then rinsed several times in a solution of 1% DMSO, 0.1% Tween 20 in PBS before incubation with the antibody. Afterward the preparations were counterstained with Alcian green and cartilages were dissected out and flat-mounted as described above.

RESULTS

Cellular Correlates of Early Cartilage Form

Cartilages of the segmented jaw, opercular, and gill-bearing skeleton of the zebrafish develop during late embryogenesis (Fig. 1A; Kimmel *et al.*, 1995; Cubbage and Mabee, 1996; Schilling and Kimmel, 1997). Most are curving bars that function as supportive devices from the time of hatching, about 3 days following fertilization, when active swimming and feeding begins. The ventrally located M cartilage (see Fig. 1 for abbreviations) in the mandibular arch and its homologue CH in the hyoid arch are the most prominent of these strut-like cartilages. A few of the cartilages also have flat, plate-like regions. The prominent dorsal mandibular and hyoid cartilages, P and HS, are complex in form. In both, a thin rod of cartilage projects anteriorly from a flat plate. Near the location where the rod and plate meet, a joint is made with the more ventral cartilage of the same arch.

The arrangements of the chondrocytes within the early cartilages are, for the most part, simple and stereotyped. Refractile (Fig. 1B), Alcian-positive (Fig. 1D) matrix is present in only a thin layer around each chondrocyte, and between the chondrocytes and the overlying perichondrium. Sectioning reveals that the cartilages, irrespective of their sizes, are generally only a single cell thick along most of their lengths (Fig. 1C). In the more slender cartilages chondrocytes are usually arranged in a one-cell-wide row, circular in cross section, just as for a neat stack of coins. Such is the case for the CB cartilages (shown in section in Fig. 1C), and for the rod-like anterior end of the HS, its SY region (Fig. 1D). Where the cartilages are larger, the chondrocytes form mosaic tile-like sheets (Fig. 1B, D). Importantly, within these sheets the chondrocytes can also form stacks, as in the SY, but in these larger cartilages several adjacent stacks lie in parallel, and also parallel to the long axis of the cartilage (Fig. 1D; CH, HM, P).

The principal feature of chondrocyte arrangement within cartilage sheets that gives the appearance of stacking is the nature of the boundary lengths between adjacent cells, as illustrated for the HS in Fig. 2. Some boundary lengths of the polygonal chondrocytes are substantially longer than others, and these are singled out in Fig. 2C. We discern the cell stacks where rows of these longer cell boundaries are aligned in parallel.

We note that cell stacks in the dorsal part of the HM curve toward the dorsal–anterior apex of the HM (toward the top in Fig. 2). This apex marks the anterior end of a prominent dorsal joint that the HM makes with the chondrocranium (Schilling and Kimmel, 1997). In contrast, the more ventral stacks in the HM do not curve toward the ventral–posterior apex (downward in Fig. 2) where the HM makes a joint with the opercular bone, but are invariably aligned with the long axis of the HM. As we show below, this patterning changes in the jaw mutants we studied.

At the ventral–anterior end of the HM, just where it is fused to the SY, is a singular region we term the "interhyal joint" (IJ) region because this is the region of articulation with the interhyal (IH, Fig. 1D). Here the chondrocytes are generally smaller than elsewhere in the cartilage (Fig. 2A) and they overlap one another, rather than being present in a one-cell-thick layer as they are elsewhere (Fig. 2B). Furthermore, IJ cells never appear stacked (Fig. 2C). Hence the IJ region has attributes that are exceptional with respect to the organization of the chondrocytes. We note that chondrocytes cells are also disorganized and overlapping in the small IH cartilage itself, adjacent to the IJ. As we describe below (see Fig. 7), patterning of the IH occurs later, during young larval stages.

However, in the HM and SY the chondrocyte stacks appear to form as the cartilages differentiate in the late embryo, rather than in the developed larval cartilages afterward, as might have been due to some secondary cellular rearrangement. With Nomarski optics one can visualize the developing SY in the live embryo at the stages when the SY is undergoing chondrogenesis (becoming Alcian-positive; Schilling and Kimmel, 1997) at about 2.5 days postfertilization. The early chondrocytes are extremely flattened along the anterior–posterior axis at this stage (Fig. 2D), which might mean they are being compressed along the SY axis (see Discussion). During the next few hours the SY cells enlarge and change in shape, becoming significantly plumper (Fig. 2E; Table 1), and the SY rapidly lengthens.

We can explain compression, and hence flattening of the early cells in the SY, by imagining that the SY develops as an outgrowth from the hyoid precartilage condensation (see Introduction), pushing out into the surrounding mesenchyme as new cells are added to its base (the posterior end of the SY, adjacent to where the IJ will form). We used lineage tracing to see if the SY might develop in this fashion. Dye labeling serves to mark individual chondrocytes in the living cartilage as landmarks, allowing us to ask upon later reexamination of the same cartilage, where, in relation to the labeled cells, new ones are added. At the first observation in the example shown in Fig. 3, three labeled cells were collected in a region about halfway along the length of the SY (Fig. 3A). In particular, the most anterior one (to the left in the figure) was 13 away from the SY's tip (the anterior end; Fig. 3A). Eight cells were posterior to the labeled group, before coming to the IJ region where the cells are not stacked. At the second observation, about a day later (Fig. 3B), 5 more cells were present in the SY, and, consistent with an outgrowth mode of development, the labeled group, still 3 cells, was still 13 cells away from the tip. The new (unlabeled) cells were all apparently added in the posterior region of the SY.

Another interesting difference between the two stages was in the arrangement and neighbor relationships among cells within the region of the labeled ones (Fig. 3C). Five unlabeled cells are present between the most anterior and most posterior labeled ones at both stages, but within this region several of the cells have more neighbors at the earlier

A
HS
CB1-4
CB5
BB
P
CH
BH
M
B
LAP
HM
C
HM
CB1
D
HM
IJ
IH
CH
SY
P

stage than later. The change, a reduction in neighbors, accompanies rearrangement of all five unlabeled cells into a single row, and is consistent with a process of cell intercalation driving the outgrowth of the SY and building the stack that eventually is only one cell wide.

Another possible means of cartilage shaping in the condensations is the selective pruning of cells by apoptosis. However, preliminary study of cell death in the hyoid condensation failed to reveal significant numbers of dying cells by Nomarski optics (C.B.K., unpublished observations), or apoptotic cells by TUNEL labeling (R. Reyes and C.T.M., unpublished observations).

Isometric Growth of the Hyosymplectic

The above analyses indicate that during the initial formation of a pharyngeal cartilage, before there is much overt growth, the differentiating cells of a precartilage condensation might be stereotypically repacked into an arrangement important for how the cartilage is shaped. The cartilages then grow during the period of larval development, before their ossifications begin (Cubbage and Mabee, 1996). Allometric (differential) growth could reshape the cartilages during this time, or they could grow isometrically, retaining their early forms. We examined the HS over a period of about a week, as an example to learn how a cartilage of complex shape can grow following its initial morphogenesis, and still maintain both its rod and plate morphologies. We observed little change in its form, either by simple visual inspection of dissected flat mounts (Fig. 4) or by various quantitative measures. During the period between 2.5 and 10 days postfertilization the surface area of the HS increases extensively, more than ninefold (Fig. 5A), and the growth rates of the rod-like SY and plate-like HM regions of this cartilage are about the same, despite their initially quite different shapes. For example, the rates of increase of the axial lengths of the SY and HM are similar (compare the slopes in Fig. 5B), as was also observed for other comparative measures not shown. The only significant difference we found in the shapes of the older versus younger cartilages is that the IJ and local region of the HM next to the IJ becomes relatively thicker, about 1.3-fold between days 3 and 8 (Table 2). An older HM also appears generally more angular (more sharply sculpted) than a younger one, as can be judged from Fig. 4. Generally, however, growth of the hyosymplectic in the young larva is nearly isometric.

The older, larger cartilages contain more cells than the younger, smaller ones (Fig. 5C), revealing that cellular addition to the early cartilages is playing a leading role in how they grow. Normalizing the change, by taking the cell number per unit cartilage area (Fig. 5D) adds two bits of information: First, the number of cells per unit area substantially decreases. The decrease shows that not all of the cartilage's growth is due to cellular addition; rather the cells are also getting larger. Whereas numbers of lacunae, rather than chondrocytes, were counted in these Alcian-labeled preparations, it is clear that the cells themselves are enlarging from measurements taken from living preparations with Nomarski optics (Figs. 2D and 2E). The enlargement is more rapid at the earlier stages, between 2.5 and 4 days, when as discussed above cell shapes in the SY are also rapidly changing (Table 1). After day 4 the increase in cell number accounts for most of the growth. Second, if one compares the data between the SY and the HM in Fig. 5D,

FIG. 1. Pharyngeal cartilages and their arrangements of chondrocytes. (A) Diagram of the segmental series of cartilages of the young larva, in a left-side view above (dorsal to the top and anterior to the left) and in a ventral view below. P and M are dorsal and ventral cartilages of the mandibular (first pharyngeal) arch (all abbreviations used in this paper are listed at the end of this legend). HS and CH are their putative homologues in the hyoid (second pharyngeal) arch. CB1-4 bear the set of four gills and CB5 (seventh pharyngeal arch) bears teeth. BH and BB are in the ventral midline (see Schilling and Kimmel, 1997 for a description of all of these cartilages and features of their development). (B) Dorsolateral surface view of the HM. Nomarski imaging in the live 5-day larva, revealing the mosaic-tile appearance of its cells. The arrow points to a nerve that passes through the hole in the HM, prominent in other figures (e.g., D), the hyomandibular foramen. Striated muscle fibers of LAP are also evident. Through-focus sectioning reveals that no chondrocytes are present above or below the plane of focus in the figure; there is only a single layer of them. (C) Horizontal Epon 7.5-μm section through the pharynx at 4 days, stained with methylene blue and basic fuchsin. Cartilage matrix is colored purple, the final magnification is the same as for B. The section passes through the HM, and through CB1–3. The HM cells in such sections have a low-columnar appearance; a view across such a plate of cartilage is rather like a view along a thinner rod of cartilage such as the SY (i.e., the view of the HM here is similar to the view of the SY in D). Sections across the rod-like cartilages, here illustrated for CB1–3, show disk-shaped single cellular profiles, revealing that the cartilages have the structure of a stack of coins or checkers. Irrespective of the form of the cartilages, or how the chondrocytes are arranged, the overlying, immediately adjacent layer of perichondrial cells is flattened onto the cartilage and forms a rather complete sheath. Perichondrial cell nuclei are more elongated and compact than chondrocyte nuclei. (D) Alcian green-stained cartilages, dissected out from a 5-day larva and flat-mounted (see Materials and Methods). The presentation shows all of the chondrocytes present in these cartilages, and their organization. They lie in rows, roughly parallel to the long axes of the cartilages (i.e., the rows run roughly horizontally in P, SY, and HM, and vertically in CH). Rows are not evident in the IJ. The method does not distort the cartilage shapes, but may disturb the articulations and the positional relationships between adjacent cartilages. Hence the *in vivo* positional relationships of these elements is better shown in A than D. Scale bars: 100 μm. Abbreviations: BB, basibranchial; BH, basihyal; CB1–5, ceratobranchials 1–5; CH, ceratohyal; HM, hyomandibular region of the HS; HS, hyosymplectic; IH, interhyal; IJ, interhyal joint region of the HS; LAP, levator arcus palatini muscle; M, Meckel's; P, palatoquadrate; SY, symplectic region of the HS.

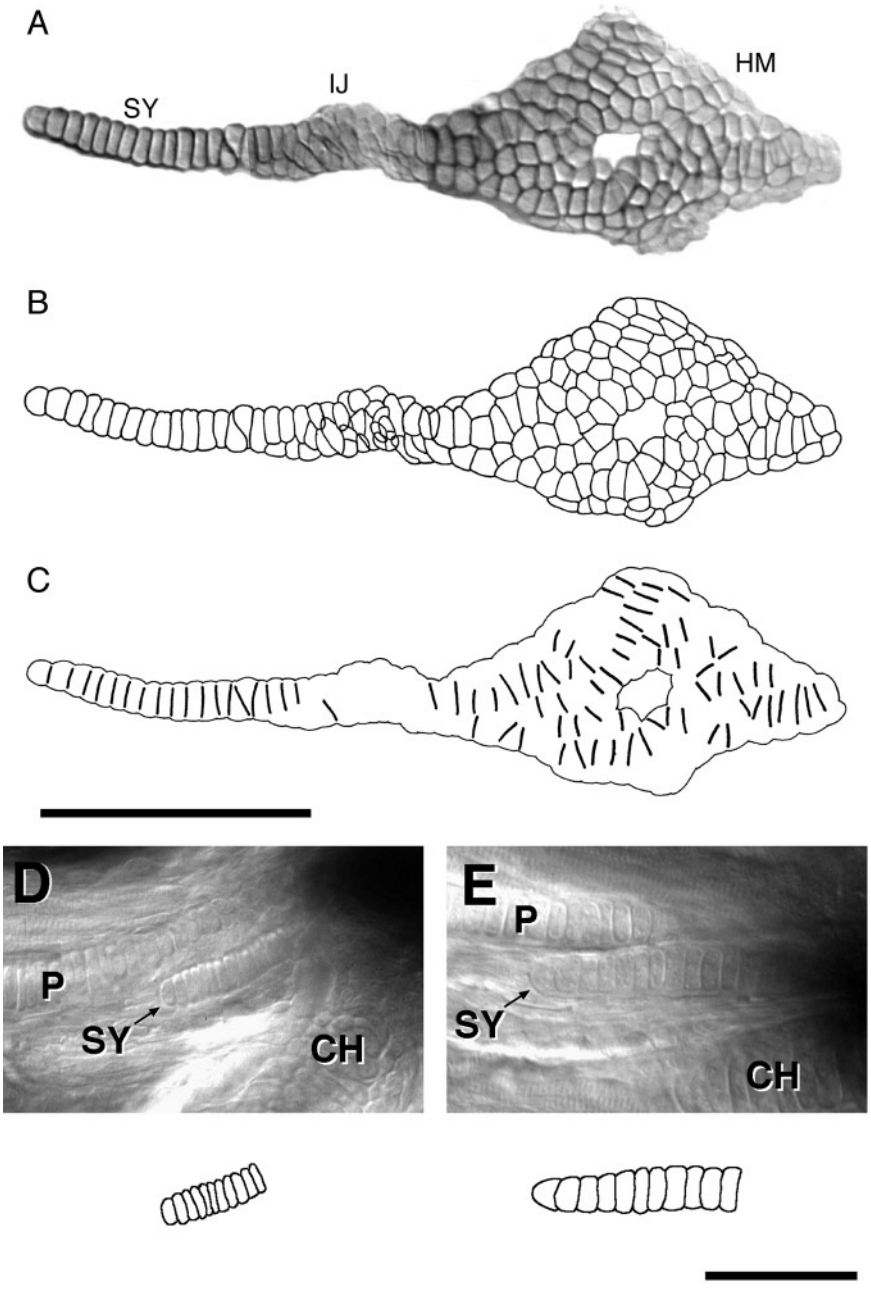

FIG. 2. Chondrocyte stacks in the young HS. (A–C) An Alcian blue-stained, dissected, and flat-mounted preparation at 3 days. The cells in the IJ are smaller and less brightly stained than elsewhere in the cartilage (shown in A), correlating with the fact that they are the last to chondrify (Schilling and Kimmel, 1997; see also Fig. 4). B shows that the IJ cells overlap considerably, in contrast to the SY and HM, where they are arranged within a single layer. They are aligned into a single row (a stack) in the anterior SY (to the left), where the cells are checker-shaped and have exactly two neighbors, ignoring the perichondrium. Closer to IJ the SY cells typically have more than 2 neighbors, as in this example. Stacked cell arrangements are also evident in the HM. The HM cells are polygonal; individual cells mostly have 5 or 6 neighbors. In C a side of a polygon is only drawn if it is noticeably longer than other sides, and if the apposition is with only a single adjacent cell. This presentation facilitates picking out the stacked cell arrangement in the HM; stacks are present where a row of long boundaries lie in parallel. The stacks run from left to right, along the long axis of the HM, and they also point upward toward the upper apex where a prominent joint is made with the chondrocranium (this apex is actually the HM's dorsal–anterior apex since the cartilage is obliquely oriented in the animal, see Fig. 1A). Note that no stacks swing downward, in the opposite direction, to the posterior–ventral apex where a joint is made with the opercular bone. These features seem invariant, whereas detailed arrangements of the cells and stacks vary considerably among different examples at the same stage (including the pair of cartilages on the left and right sides of a single individual). Scale bar (A–C): 100 μm. (D, E) Nomarski views of the SY in a live embryo at 65 h and a live larva at 97 h postfertilization. The arrow points to the anterior end of the SY cartilage, its left end in the figure. The accompanying drawings outline SY cells, reconstructed from multiple focal plane Nomarski images. At the earlier stage (D) the cells are coin-shaped; within a few hours they plump into a puck-shape. By 97 h (E) the cells have enlarged considerably; the increase in area in the plane of view is about 2.7-fold. Scale bars (D, E): 50 μm.

TABLE 1
Change in Young Chondrocyte Shape and Size in the Developing SY

Group	n^a	Height[b]	Width	Ratio[c] (height/width)
65 h	20	10.9 ± 0.8	2.8 ± 0.5	3.9 ± 0.9
70 h	20	11.3 ± 1.0	4.3 ± 0.7	2.6 ± 0.6**
97 h	30	14.4 ± 1.3	5.7 ± 0.8	2.5 ± 0.5**

[a] Counting from the anterior end of the SY, cells 2–11 were measured from each of two animals for the 65- and 70-h time points, and from three animals at the 97-h time point. In all of the cases the measured cells had two neighboring cartilage cells, one to either side of it, no more or no less (the most anterior cartilage cell was excluded because it always has only a single chondrocyte neighbor).

[b] Height is the dimension of the cell perpendicular to and width is the dimension of the cell parallel to the long axis of the SY, in μm (mean ± SD). The measurements are from Nomarski photomicrographs (40× objective, as in Figs. 2D and 2E) taken from living whole animals to avoid artifactual cell shape changes due to fixation and staining.

[c] Probabilities were determined from Student's *t* test. **The difference between the ratio at 65 and 70 h or 97 h is highly significant ($P < 0.001$). The difference between 70 and 97 h is not significant at the 5% level.

one finds no difference in either the number of cells per unit area, or how this relationship changes with development. The finding suggests that differential control of cell size does not appear to be involved in the different rates of growth expressed by the rod- and plate-shaped regions of the same cartilage. The difference is explained by faster cellular addition to the HM (Fig. 5C).

Additionally, isometric cartilage growth does not appear to require exact, stereotyped placement of the newly adding cells. As the SY becomes both thicker and longer, the single cell stack that initially makes up much of its length gives way to an irregular and variable pattern of cell arrangement. Figure 6 compares, in flat mounts, cellular organizations in left and right pairs of the anterior region of the SY at day 8, and Fig. 7 shows sections through the SY in a single individual. Clearly, at this advanced larval stage the locations of boundaries between cells in the SY are variable. In the anterior SY in particular we see cell doublets where single cells were stacked earlier, highly suggestive that the chondrocytes present in the early cartilage have divided. A cell in a nearby cartilage captured in late mitosis is shown in Fig. 7C (arrow), proving that chondrocytes are indeed capable of mitosis at this stage. As is well shown in Fig. 7A, the nuclei in the SY cell pairs usually lie opposite to one another, making a double row along the cartilage, but the cell boundaries can be either orthogonal, relative to the nuclear positions (such that the cells appear stacked as in the left part of the SY in Fig. 7A) or oblique (as to the right). Cell arrangements are rather more variable in the posterior SY (Figs. 7B and 7C).

A detail of interest is the arrangement of cells at this advanced stage in an adjacent cartilage, the IH, shown in Figs. 7B and 7C. The IH chondrocytes are organized in a short row oriented vertically in the figures. At younger stages, as noted above, the IH is a small, rather shapeless mass and its cells are multilayered and unstacked, not forming a single layer as we see here. Reconstruction of this and other examples reveals that by day 8 the IH cartilage has taken the shape of a small plate, one cell thick, and oriented transversely in the larva where it can serve to buttress the CH. Two points arise from this observation: First, since the IH was well chondrified earlier (Fig. 1D), we see that significant reshaping of a cartilage element can occur after its initial chondrification. Second, we cannot conclude that because some pharyngeal cartilages grow isometrically during particular stages of development (e.g., the SY and HM) all of them are behaving similarly. What is a period of isometric growth for the HS is a period of shape change for the IH.

We used BrdU labeling of the young cartilages to learn how cell divisions contribute to cartilage growth. Exposure to BrdU between 2 and 3.5 days yielded little or no labeled cells in pharyngeal cartilages, although other tissues in the embryo were well labeled (data not shown). However, chondrocyte nuclei were well labeled after exposure to BrdU beginning at 3.5 days, and afterward at 4–5 days (Fig. 8). We observed that the number of labeled nuclei present in individual cartilages varied considerably. Generally the older cartilages showed more labeled cells, and exposure for longer periods (24 h vs 0.5 h) also resulted in increased labeling. In cases where exposure was less than 4 h, we invariably observed only single nuclei labeled within individual lacunae. Exposure for 4 h or longer resulted in labeling of not only single nuclei, but also pairs of smaller nuclei labeled side-by-side within a single lacuna (arrowheads in Figs. 8A and 8B), suggesting that the side-by-side cells are newly divided mitotic sisters and that cellular addition to the cartilage occurs by divisions of the chondrocytes themselves. However, the divisions do not occur uniformly along the

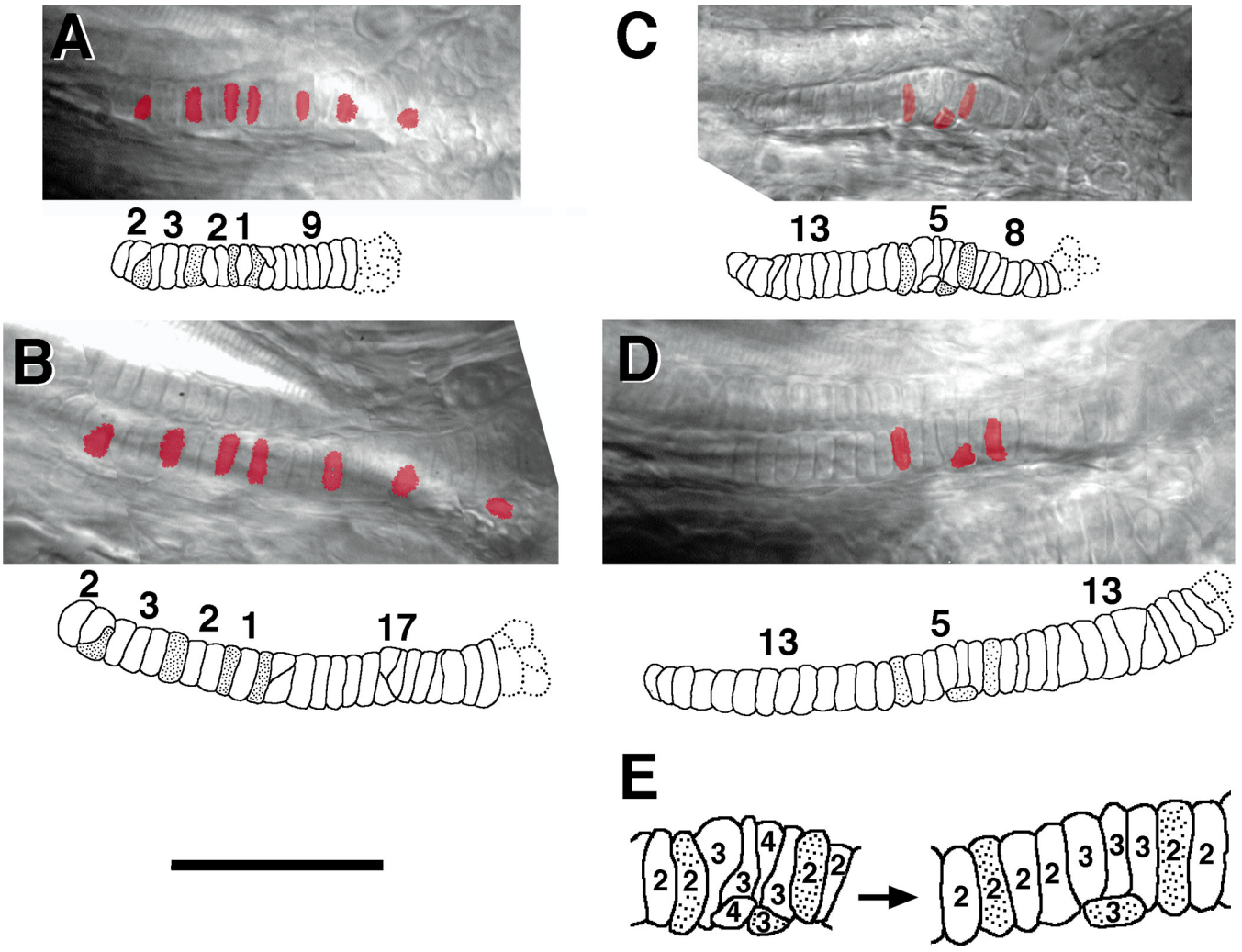

FIG. 3. Formation of the SY cell stacks. Two examples (A and B, C–E) are shown. Cells were labeled in the early embryo, by injection with rhodamine–dextran (see Methods and Materials) and the SY, when containing labeled descendants of the injected cells, was photographed in the same two live larvae at 3 days (A, C) and 4 days (B, D) of development. The micrographs show overlays of single-plane images of epifluorescence (with fluorescent labeling pseudo-colored red) and with Nomarski bright-field illumination through the same SY cartilage at the two stages. Anterior is to the left. The accompanying drawings show the SY cell stack reconstructed from the multiple focal plane Nomarski images, with the labeled chondrocytes stippled. In A and B the three labeled cells to the right are perichondrial cells, not chondrocytes, and they are not included in the drawings. The numbers show how many unlabeled cells are distributed along the cartilage relative to the positions of the labeled ones. The dotted cell outlines to the right show a few of the unstacked cells present in the IJ. Between the two time points unlabeled cells add preferentially to the posterior SY (to the right) in these examples, and in another case analyzed similarly. (C) An enlargement of the local region including the labeled cells in the second larva. The number within each cell indicates the number of chondrocyte neighbors it contacts. Less contacts are made at the older stage, presumably due to cellular intercalations occurring between the two times, and that make the more orderly stack at the later time. Scale bar: 50 μm for A–D, 25 μm for E.

HS (Fig. 8C). The SY, IJ, and HM adjacent to the IJ are regions of dense labeling. There is a large central zone within the HM where cells do not divide, and within the more peripheral regions of the HM cells near the dorsal–anterior apex (upper in Fig. 8C) appear to be dividing much more rapidly than those near the ventral-posterior apex (lower).

Hyoid Cartilage Shapes in sturgeon, schmerle, and sucker Mutants

Study of mutants in which cartilages are incorrectly shaped provides a direct way to learn the roles of specific genes in cartilage patterning. We examined three mutations, *sturgeon* (*stu*$^{-}$), *schmerle* (*she*$^{-}$), and *sucker* (*suc*$^{-}$),

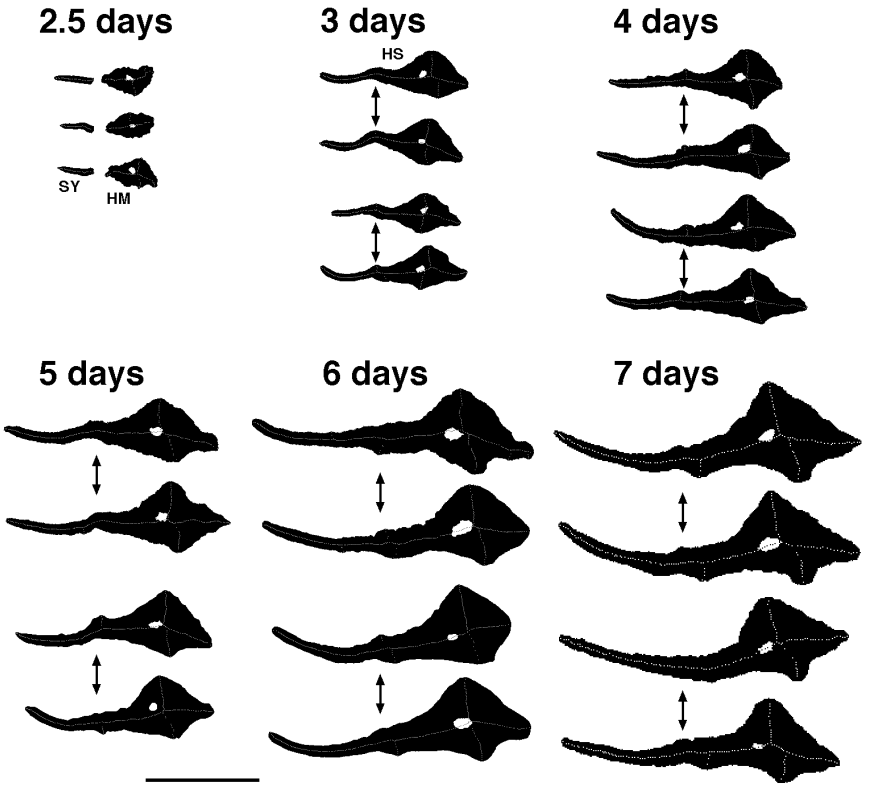

FIG. 4. Growth of the HS does not change its shape. The silhouettes were made from Alcian blue- or green-stained, dissected flat mounts. Double-headed arrows point out the IJ regions of left–right HS pairs taken from single individuals. In the other cases only a single cartilage, either the left or the right, was prepared from an animal. The dots within each silhouette were generated by a computer algorithm that finds the geometric centers (middles) of local regions of cartilage. The set of these centers forms a curve, the "symmetric axis" of the structure (Weber and Blum, 1979), from which a number of measures can be made. For example, we measured along the length of the main segment of the symmetric axis to compute the growth in length of the SY and HM (shown in Fig. 5B). At the earliest stage (2.5 days), the SY and HM are chondrifying separately. They fuse together at the IJ region to form a single element (the HS) by the next stage (3 days), and during the next several days the cartilage grows rapidly without substantial change in form. Scale bar: 200 μm.

characterized as producing cartilage deformations specifically in the first two pharyngeal arches (Piotrowski *et al.*, 1996). The joints between the dorsal and ventral cartilages in these arches (i.e., the joint involving the HM, IH, and CH in the hyoid arch) are missing in all three mutants. Additionally, all three share a phenotypic similarity in that the more ventral cartilages (in the hyoid arch, the CH, IH, and/or SY, in contrast to the dorsal HM) are variably reduced, with the loci making a quantitative series with respect to severity of this disturbance: $stu^{-} < she^{-} < suc^{-}$ (Piotrowski *et al.*, 1996). We extended the previous study by examining dissected and flat-mounted cartilage preparations that more clearly reveal the nature of the changes in cartilage shapes. Focusing on the hyoid arch, we observed a large variety in the shapes of the mutant cartilages, and to try to make sense of these changes we compared the cartilages grouped not strictly by genotype, but as arranged in Fig. 9 where we show them in a series that is based on how much hyoid cartilage we find in a given mutant larva. Remarkably, not only is less ventral cartilage present as the series progresses (as we expected from the analysis of Piotrowski *et al.*, 1996), but we also can follow what appears to be a pathway of change in shape:

In none of the examples do we observe a cartilage or region of cartilage recognizable as the equivalent of the wild-type IH. An IH might have been distinctive by position and shape of neighboring elements, even if the IH were partially fused to them. In contrast, in every example and in spite of the considerable variability, we can circumscribe a cartilage region that resembles a wild-type HM of approximately correct shape and size. The figure legend adds detail about why we identify this mutant HM region as we do. In the most severe members of the series (last examples in Fig. 9) the mutant HM region comprises nearly all of the hyoid cartilage that is present in the hyoid arch (although, as did Piotrowski *et al.*, we observe in many of these mutants ectopic cartilages of unrecognizable identities; e.g., Fig. 9H, >).

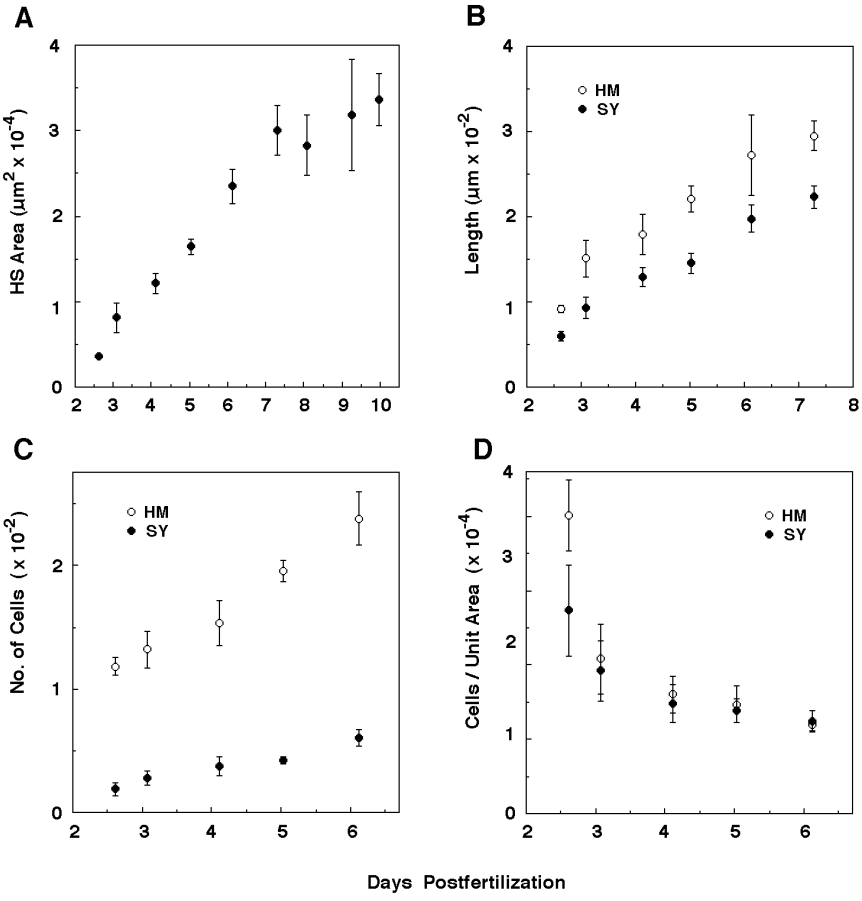

FIG. 5. Quantitative features of HS growth. These data show means ± standard deviations, taken from cartilages prepared as shown in Fig. 4, and including cartilages at days 8–10 not shown there. At least 3 cartilages (usually 6–8) were measured for each time point. (A) Surface area, as estimated by a computer-generated count of the number of pixels included in the silhouettes shown in Fig. 4. This measure ignores any growth in the third dimension. (B) Lengths of the HM (open circles) and SY (closed circles) regions increase at about the same rate. Lengths were computed from the major segment of the symmetric axis of the HS (see legend to Fig. 4), shown as the row of dots running from left to right in Fig. 4. For the purpose of these measurements we arbitrarily but consistently divided the HS into the SY and HM regions just at the estimated center of the IJ. The double-headed arrows in Fig. 4 show examples of the point of subdivision; typically at the IJ there is an abrupt change in thickness. In some cases (e.g., the 3rd cartilage in the 7 day group; Fig. 4) we used the IJ's characteristic cell size and arrangement (see Fig. 2) to locate it. (C) Cells rapidly increase in number in both the HM and the SY during growth. The cell counts were made from the Alcian-stained preparations themselves, not from micrographs because focusing through the preparation aided in obtaining an accurate cell number, particularly in the IJ where the cells are overlapped (see Fig. 2). The data extend only through day 6 because afterward the increase in cells in all regions precludes accurate counts. The method, counting lacunae (i.e., an Alcian-stained cell-chamber) in Alcian-stained preparations, underestimates the actual number of chondrocytes because at and after day 4 newly divided sister-cell pairs of chondrocytes occupy single lacunae. (D) Cells per unit area decrease at about the same rate in the HM and SY. Although there is some thickening of the cartilage matrix, chondrocyte enlargement (Figs. 3D and 3E) contributes primarily to this change, mostly occurring before day 4.

We can also recognize a region clearly corresponding to the SY, topologically in the correct location relative to the mutant HM region, but present only in the least severe members of the series. The mutant SY region can approach the wild type in shape and size (Fig. 9B), or can be substantially reduced and misshapen (Fig. 9F). What could be an SY, but reduced to a simple nub of cells, can be seen in several examples much later in the series (e.g., ,Fig. 9K, triangle).

Perhaps the most interesting are changes through the series that we propose relate to the region developing the CH. Following the series, the anterior tip of a clearly recognizable mutant CH region (*, Fig. 9E) would appear to correspond to a short string of ventral and anterior cartilage in examples further along (*, Figs. 9G and 9I), and then, near the end of the series, to a small clump of cartilage located on the ventral and posterior region of the HM (*, Fig. 9N).

The cellular organization associated with this apparent polarity change (see Discussion) is also revealing: A ventral

TABLE 2
Growth in Thicknesses along the Anterior Elongated Part of the Developing HS

		Thickness[a]		Ratio[b]		
Group	*n*	SY_a	SY_p	IJ and HM	SY_p/SY_a	IJ and HM/SY_1
Day 3	8	11.6 ± 0.8	14.5 ± 1.6	22.1 ± 3.4	1.25 ± 0.13	1.91 ± 0.35
Day 6	6	14.6 ± 0.8	21.6 ± 2.4	39.3 ± 2.6	1.48 ± 0.22*	2.71 ± 0.28**
Day 8	5	18.9 ± 1.0	23.9 ± 4.8	48.1 ± 3.2	1.28 ± 0.28^{ns}	2.55 ± 0.19**

[a] Thickness is the average diameter (μm ± S.D) for each cartilage from a series of computer-aided measurements (at least 20 in each individual case) along the anterior half of the SY (SY_a), the posterior half of the SY (SY_p), and the local region including the IJ and HM just adjacent to it (IJ and HM, see text). For the sake of consistency, we made the HM measurements along just $\frac{1}{3}$ of its entire length.

[b] Probabilities were determined from Student's *t* test. *The difference between the ratio at day 3 and the ratio at day 6 is marginally significant ($P < 0.05$). **The difference between the ratios at day 3 and days 6 or 8 is highly significant ($P < 0.01$). ns: the difference between the ratios at day 3 and 8 is not significant at the 5% level. Also, none of the changes in ratios between days 6 and 8 are significant at this level. The notable change is in the thickness of the IJ and HM. Relative to the growth of the SY_a the difference is 1.3-fold over the period (2.55/1.91 = 1.3).

wedge-shaped region where cartilage is present but thinned out occurs in the middle of the series (arrowhead, Figs. 9I and 9K). We can suppose this thinned region to correspond to that of less severe examples where the ventral cartilage mass is "pinched off" from the HM (arrowhead, Figs. 9E and 9G). The pinched region would appear to correspond to the location of the dorsoventral joint and the IH in the wild type. Chondrocyte rows curve into the ventral cartilage mass, or string, never from the posterior part of the mutant HM, but invariably from its anterior part (arrrows in Figs. 9K and 9L; see also 9J). By our interpretation these rows curve from the mutant IJ region ventralward to the location where the joint would normally be made.

This interpretation of the *suc* mutant phenotype in the hyoid arch, in which a substantially diminished CH region is fused with reversed polarity to the ventral region of the HM corresponds to that of Piotrowski *et al.* (1996) for the mandibular arch. They proposed that in *suc* mutants a reduced Meckel's cartilage (the putative CH homologue) is fused to the ventral part of the palatoquadrate (the putative HM homologue). We confirm these changes in the mandibular arch (Fig. 10), and note that by our interpretation of the defect in the hyoid arch (i.e., reduction of the CH and its fusion to the HM as shown in Fig. 10), changes of just the same nature occur in both arches. Whereas, in both arches, the dorsal and ventral cartilages are invariably fused together (due to the joints being missing) we note that in spite of the close association of the mandibular and hyoid arch cartilages apparent in the figure there is never a cartilage fusion at this location: the joint made between cartilages of the two arches is present as is the case in wild types.

DISCUSSION

The findings presented here suggest that after the precartilage condensation forms in the embryo, development occurs in two distinct phases. First there occurs a period of rapid cartilage morphogenesis that accompanies chondrocyte differentiation (Schilling and Kimmel, 1997). We propose that as the cells first deposit matrix, their divisions are unimportant and cell rearrangements that form stacks play a leading role in shaping the elements. Second, there is an extended period of cartilage growth. Growth involves regulated cell divisions, but control of local cell arrangement now seems less important, even as the cartilage grows isometrically, i.e., without change in form. Hence, cellular behaviors during these distinctive phases of morphogenesis and growth seem to be governed by two different sets of rules. Analysis of jaw-deforming mutations has provided an entry for understanding the first set.

Stacks of Chondrocytes

Other authors have also noted that chondrocytes can be aligned into stacks, e.g., in the developing cartilage models of long bones, including the digits, in limb buds, and in other cases as well (Bertmar, 1959; Wood, 1982). The underlying cellular behaviors might differ in separate instances. For example, hypertrophic chondrocytes are frequently stacked within the epiphyseal plates of long bones, and these "isogenous groups" might represent clones deriving from oriented mitoses (Thorogood, 1983). However, the stacks we observe appear at stages when we could not detect cell divisions by BrdU labeling. Moreover, in one instance (Figs. 3C–3E) we observed local changes in cell–neighbor relationships that are consistent with the cell row forming by oriented cellular intercalations that would elongate the developing SY in the same fashion that oriented intercalations underlie elongation of the notochord (Shih and Keller, 1992). The cellular behaviors mediating intercalations may be driven by changes in cell adhesions (Irvine and Wieschaus, 1994).

Our vital dye-labeling evidence also suggests that the SY

grows out from the condensation from one end to the other, i.e., that stack building is a polarized process. A sheet of cartilage cells, as found in the HM, behaves mechanically similarly to an epithelium (Honda, 1983); and like epithelial cells, chondrocytes might be fundamentally polarized (Trelstad, 1977). If so, cell polarity could contribute to polarized cartilage outgrowth. Cells appear to add to the developing SY from its posterior end where the IJ also develops, the singular region in which the cartilage cells are not detectably stacked. This view is consistent with previous evidence (Schilling and Kimmel, 1997) that when Alcian labeling can first be detected in the SY (at about 53 h postfertilization), only one or a small cluster of SY cells is labeled, located just across the presumptive IJ from the positions of other chondrifying cells forming the HM and the CH (see also Bertmar, 1959). The IJ neighborhood thus appears to serve as a generative or patterning region for both morphogenesis and chondrification.

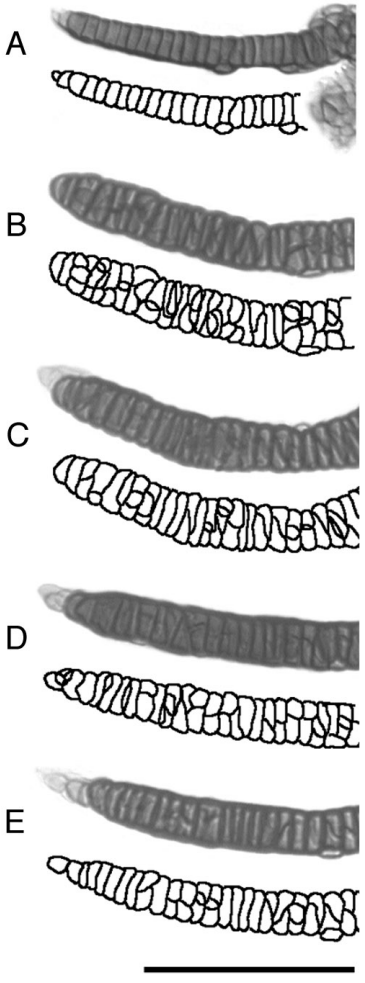

FIG. 6. Disruption of the SY cell stack during growth. Alcian green-labeled flat mounts, and accompanying tracings of the chondrocyte outlines. (A) An example at day 4. The SY cells are neatly stacked (compare with other examples in Figs. 1D, 2, and 3). (B, C) and (D, E): The left–right pairs of two larvae at day 8. Cellular addition variably disrupts the early stacks. The cells in many regions are substantially overlapped. Scale bar: 100 μm.

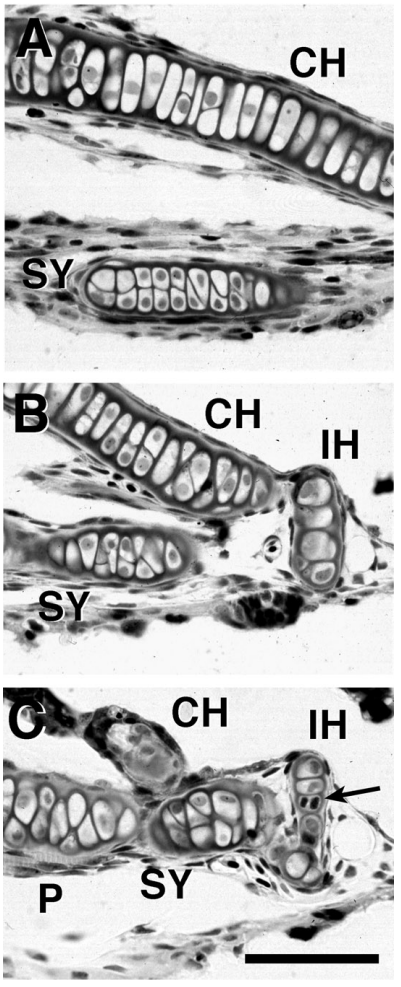

FIG. 7. Chondrocyte arrangements in advanced larval cartilages. Horizontal 5-μm Epon sections through the pharynx at day 8, stained with methylene blue and basic fuchsin. The sections were selected from a serial series running ventral (A) to dorsal (C). Anterior is to left and medial is to the top. Chondrocyte cytoplasm is pale, such that the dark cell appositions and nuclei are prominent. Note the thin perichondrial layer around each of the cartilages and the chondrocyte in late telophase (arrow in C). Scale bar: 50 μm.

The change we observed in SY cell shape (Figs. 2D and 2E) during its morphogenesis also might be related to stack formation. A variety of explanations can be envisaged for why chondrocytes are flattened in newly emerging cartilages, and among them are mechanical ones. Arguing from first principles, Thompson (1942) showed that soap bubbles arranged in a string (i.e., arranged like the chondrocytes in

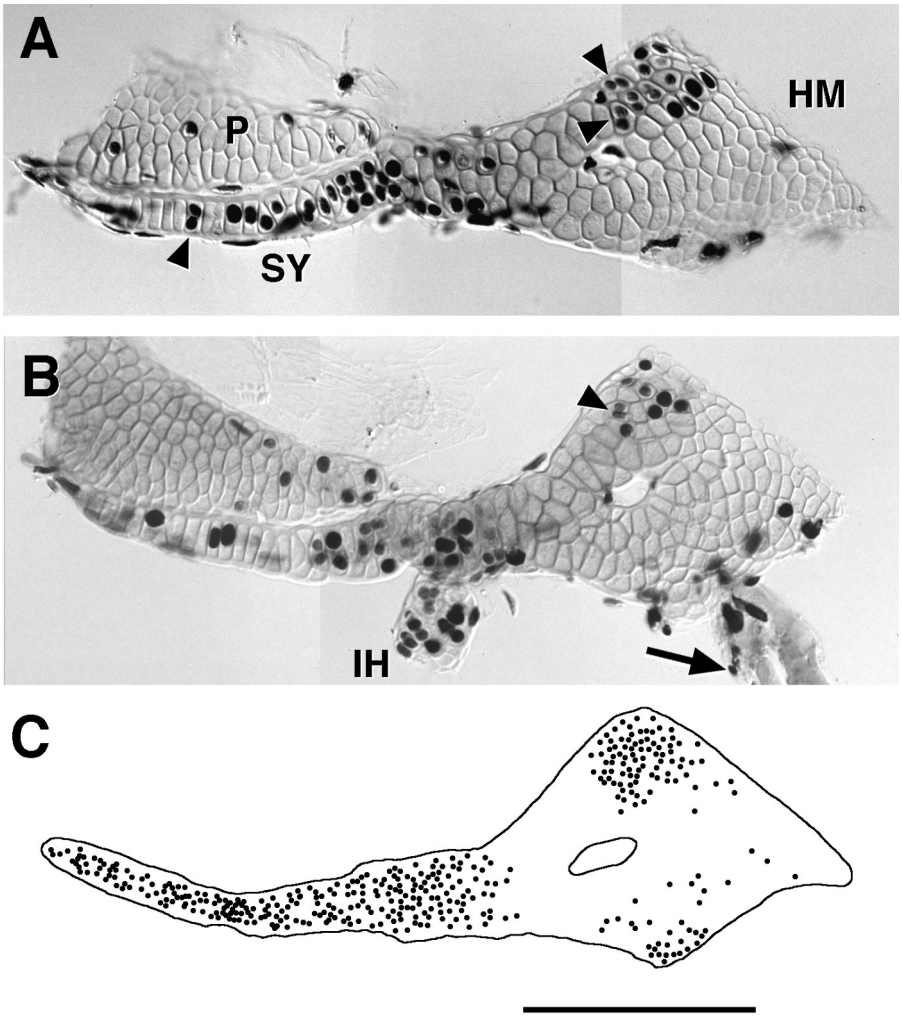

FIG. 8. Bromodeoxyuridine labeling of the growing HS. (A, B) Two examples at day 4.5, after exposure to BrdU for 1 day (and refreshed at 6-h intervals), counterstained with Alcian green. Labeled round-shaped nuclei are chondrocyte nuclei, whereas the thin elongated nuclei are of mesenchymal perichondrial cells. Arrowheads show examples of pairs of small labeled chondrocyte nuclei present together in a single lacuna, probably representing the pair of daughter cells stemming from a single mitosis that occurred during the day-long exposure. Examination with Nomarski optics confirms that the two nuclei are within separate cells that had not yet formed an intervening Alcian-positive matrix. We did not observe such pairs if the labeling time was less than 4 h, even though many single labeled nuclei were present (data not shown). This would mean that 4 h is about the minimal time that it takes for a chondrocyte captured by BrdU incorporation in the S phase of the cell cycle to have completed that cell cycle and divided (i.e., 4 h is approximately the length of the G2 + M phases of the cell cycle). In B labeling is also present in the IH and in cells overlying the forming opercular bone (arrow), which articulates with the HM's ventral–posterior apex. (C) The location of every labeled chondrocyte nucleus in 12 cartilages, exposed to BrdU as in (A, B) is plotted on a single overlay, revealing that the distribution of labeling is markedly nonrandom. The central region of the HM is practically devoid of labeled chondrocytes, showing it to be a region where the cells are not dividing. Quantitative analyses (not shown) reveal that significantly more labeled cells occupy the region of the HM's dorsal–anterior apex (to the top) than its posterior–ventral apex (to the bottom; $P < 0.001$; t test). This finding suggests that chondrocytes are dividing more rapidly in the dorsal–anterior apical region, since there is no difference in how tightly the cells are packed within the two regions. The IJ, the region of the HM adjacent to it, and the SY are also regions where cells appear to be dividing at a relatively high rate. Scale bar: 100 μm.

the SY stack) will, due to their surface tensions, have a height (dimension across the string) twice their width (dimension along the string). We found that when the SY chondrocytes are first differentiating, the height:width ratio was much higher than the Thompson theory predicts (nearly 4 rather than 2 at 65 h postfertilization; Table 1). The cells then reshape toward the predicted value within only a few hours. Were the SY growing outward from the

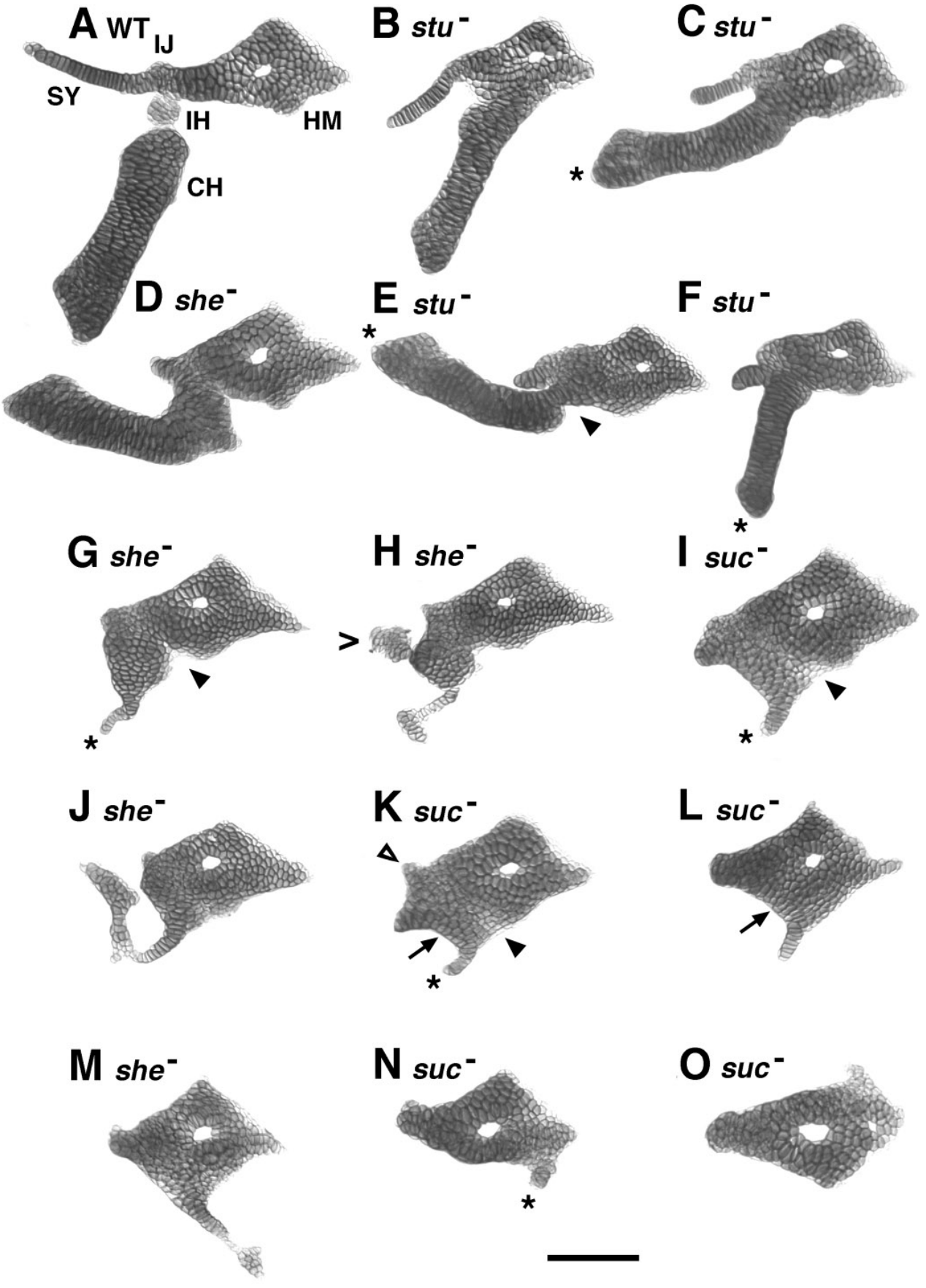
A WT IJ
SY
IH
HM
CH
B stu-
C stu-
D she-
E stu-
F stu-
G she-
H she-
I suc-
J she-
K suc-
L suc-
M she-
N suc-
O suc-

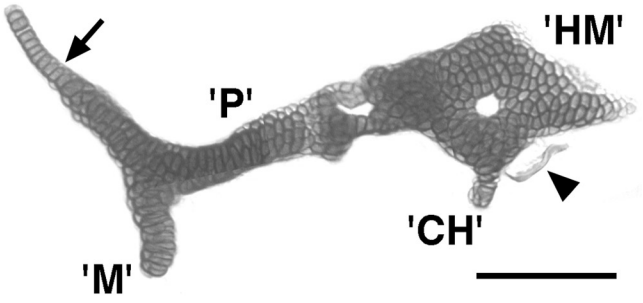

FIG. 10. A similar *suc*$^{-}$ phenotype occurs in the mandibular and hyoid arches. Flat-mounted dissected preparation at day 5. There is tight apposition, but not a fusion, between the cartilages that we identify as the mutant equivalents of the dorsal segmental homologues, P in the mandibular arch and HM in the hyoid arch. The apposition between them is topologically as in wild types; occurring just where the SY normally would be present (Fig. 1). The palatoquadrate possesses a pterygoid process that appears normal in form (arrow). The ventral segmental homologues, M and CH, are drastically reduced and are fused to the dorsal elements at about the locations where the dorsal–ventral joints should occur in both arches, but which are missing in both. A small fragment of bone is present beside the posterior–ventral surface of the HM (arrowhead), about the region where the opercular bone normally develops. Scale bar: 100 μm.

condensation in the manner we envisage, its cells might be at first compressed along the SY axis, accounting for the initially high ratio.

We infer from our observations that stacks emerge as orderly cellular arrays from earlier relatively disorderly ones, but we have no direct evidence that this is the case. How cells are arranged in the precartilage condensations has never been adequately examined, although this phase of development has been a focus of attention for some time (Thorogood, 1983; Hanken *et al.*, 1992; Hall and Miyake, 1992). Thorogood (1983) has speculated that cell arrangement in the condensation is ordered and is under developmental control. A clear direction that emerges for future work is to watch the development of precartilage condensations under conditions where one can keep track of the detailed behaviors of its individual cells. We have been unable to visualize the cells adequately in the living condensations *in situ* with Nomarski optics; the cells are too many and too densely packed. Newer methods of dye labeling and imaging may allow progress in this area (Cooper *et al.*, 1997).

Distinctive Cellular Behaviors during Cartilage Morphogenesis and Growth

Following the period of morphogenesis, a phase of rapid cartilage growth occurs in the early swimming and feeding larva. For the HS the growth is nearly isometric, i.e., occurring without a substantial change in shape. The growth of other specific cartilages might be either isometric or allometric: e.g., during the same stages Meckel's cartilage grows longer and relatively thinner (unpublished observations, C.T.M), and the IH flattens into a small plate (Fig. 7).

Growth of the HS closely follows morphogenesis—most likely the two periods overlap in the newly hatched larva (ca. 3.5–4 days postfertilization). The growth rate of the HS is approximately linear at this stage (Fig. 5A); i.e., we detect no change in growth rate that would signal the changes we observed in cell behaviors. Subsequently, cells stop enlarging (Fig. 5D) and begin to divide. Whereas the morphogenetic period takes only a day or so, the growth period continues for many days. Figure 5A shows the rate of growth slowing after the first week, but we note two caveats: First, the variance increases (error bars in Fig. 5A). Second, cartilage growth depends on how well the larvae are feeding (unpublished results, and see Methods and Materials): At the extreme the HS does not grow at all between

FIG. 9. A phenotypic series in the shapes of mutant hyoid cartilages. Flat-mounted dissected preparations from *stu*, *she*, and *suc* mutants at day 5, arranged according to how much hyoid arch cartilage is present. A wild-type preparation is also included (A). The highly variable *she*$^{-}$ phenotype overlaps both *stu*$^{-}$ and *suc*$^{-}$. Two *she*$^{-}$ examples (G, H) fall in the middle of the series. Another (D) fits ahead of *stu* mutants, and two (J, M) fit after one or more *suc*$^{-}$ examples. Our interpretation of the identities of particular regions of cartilage is explained in detail in the text. In contrast to disruption of the ventrolateral hyoid (CH, IH, SY) cartilages, the dorsal HM region is readily identifiable and reasonably normal in shape and size in every mutant we examined, even though it is nearly invariably fused to other cartilages. The assignment is based on the following features, shared with the HM in wild types: The mutant HM is present as a diamond-shaped region of cartilage that articulates with the otic capsule at its dorsal–anterior apex. The HM is located just posterior to a cartilage we interpret to be its mandibular arch homologue, the palatoquadrate (e.g., as shown in Fig. 10). Muscles insert to the mutant HM that from their origins on the chondrocranium seem to be the correct ones (see Schilling and Kimmel, 1997). The mutant HM invariably has a central hole, corresponding to the wild-type hyomandibular foramen. Finally, the mutant HM is often associated with a bone primordium we interpret to be the opercular, at a posterior–ventral apex of the HM as usual (example in Fig. 10). In all three mutants, ectopic small cartilages of unknown identity are often present (H; >), emphasizing the need for region-specific molecular markers that are only beginning to become available (Schilling, 1997). Asterisks (C, E, F, G, I, K, N) indicate the position we take to be the tip of the mutant CH. The triangle (K) indicates a stub of cartilage corresponding in position to the SY. Arrowheads (E, G, I, K) indicate where we propose the joint between the HM and the CH would normally form. Arrows (K, L) show chondrocyte stacks curving ventrally from the IJ. Such curving cell stacks are also present in other mutants in this part of the series (e.g., J) but are never observed in wild types (e.g., Fig. 2). Scale bar: 100 μm.

days 4 and 11 in unfed larvae. Hence with improved rearing conditions rapid growth of the cartilages might continue longer.

Growth regulation must occur at least in part via control of the cell cycle (Bryant, 1996). Clearly, divisions are contributing more cells to particular regions of the HS than to others (Fig. 8C). We note that all of the regions that contain many BrdU-labeled cells, including the dorsal–anterior apex of the HM, the IJ, the length of the SY, and the ventral–posterior apex of the HM, are where articulations are made with other cartilages, or in the last case, with a bone (see legend to Fig. 1 and Schilling and Kimmel, 1997). Hence articulations might generally be growth zones. Further, our observation of labeled-cell doublets after longer exposures to BrdU shows that chondrocytes in these joint regions are themselves dividing (rather than newly divided cells joining the population from outside the cartilage).

During the SY's isometric growth the stacked arrangement of its cells becomes obliterated. The change is at least in part due to local variability in the orientations of sister-cell pairs after mitoses (see Fig. 7A). We think that this fine-grained disorderliness is revealing a major difference in developmental controls of organogenesis during the periods of morphogenesis and growth. We proposed above that cellular stacking is an essential ingredient in the initial shaping of the element, and now we see that during growth the stacks can be disrupted without disrupting cartilage shape. The change emphasizes that early stack building is not simply a "generic" (see Newman and Comper, 1990) property of the way cartilage cells assemble, i.e., the only possible way due to some physical or chemical cell–cell or cell–matrix constraints within the system.

Three Genetic Loci Might Act along the Same Pathway of Ventral Cartilage Morphogenesis

Rapid progress is being made in the molecular characterization of the diverse kinds of genes that play key roles in patterning the skeleton (e.g., Gendron-Maguire *et al.*, 1993; Kurihara *et al.*, 1994; Qui *et al.*, 1997; Rijli *et al.*, 1993; Yamada *et al.*, 1995; Rivera-Perez *et al.*, 1995; Subramanian *et al.*, 1995). Learning what cellular processes are controlled by these genes provides an important avenue for future work. Molecular characterization of genes first identified by mutation in the mouse has led to the exciting discoveries that proteins of the TGF-β superfamily, secreted growth and differentiation factors, function in specific precartilage condensations to control the patterning of cartilages deriving from these condensations (Kingsley *et al.*, 1992; Storm *et al.*, 1994; Storm and Kingsley, 1996). Thus the protein GDF5 is normally produced at the early sites where joints will be made between developing digits, and if this protein does not function, the joint is not made. The mutations we have examined also eliminate a joint between elements that normally articulate. Moreover, the most severe mutant phenotype we encountered (i.e., in *suc*$^{-}$) is similar to that of mouse mutants lacking function of any of three genes encoding components of an endothelin-1 signaling pathway that functions upstream of the homeobox gene *goosecoid* (Kurihara *et al.*, 1994; Clouthier *et al.*, 1998; Yanagisawa *et al.*, 1998). Our studies confirm and extend the work of Piotrowski *et al.* (1996) who observed that the *stu*, *she*, and *suc* mutant phenotypes vary substantially, and that, among the three loci, *stu* mutants have the least severe phenotypes and *suc* mutants the most severe. Further, they also reported that the CH in *stu*$^{-}$ and *she*$^{-}$ develop with a reversed anterior–posterior orientation. In our interpretation of the *suc*$^{-}$ phenotype, a small remnant of the CH is fused to the HM, and the CH points the wrong way in *suc* mutants as well. Seeing the same kind of change in all three mutants, a reversal of anterior–posteror polarity of the ventral cartilage (i.e., the CH in the hyoid arch) suggests that loss of function at any of the three loci disturbs the same developmental process, a process that we would speculate sets up a course of morphogenesis of the ventral cartilages. As we interpret the phenotypic series we described in Fig. 9, this reversal occurs in a graded way through the series (shown by the changing location of the asterisks in Fig. 9, and cartooned for the sake of clarity in Fig. 11A). Reversal is rather complete in mutants exhibiting the severest phenotypes in terms of cartilage reduction, but is only partial in intermediate members of the series. An intriguing possibility for the basis of the reversed polarity is suggested by the abnormally curving rows of chondrocytes in these intermediate examples (arrows in Figs. 9K and 9L). We argued above that normally the SY appears to form by a polarized stacking of chondrocytes. The SY stack comes from the region that also forms the joint, the IJ. We know that this region is severely perturbed in the mutants for the joint is never made in any of them. Hence, if we generalize a process that seems to be building the SY to the other cartilage regions developing from the same condensation, and adjacent to the same joint (Schilling and Kimmel, 1997), then a direct inference from these findings is that the change in cartilage polarity in the mutants is caused by their cellular stacks assembling in an incorrect orientation, from anterior to posterior in the most severe cases, rather than from posterior to anterior (Fig. 11B). The hypothesis motivates study of the precartilage condensations in these mutants and predicts that for normal development, function at any of these loci is critical before or during the process of stack assembly that begins at a late stage within the condensations.

We suppose that a patterning process similar to that in the hyoid arch also occurs in the mandibular arch, since the mutations similarly affect both arches (Piotrowski *et al.*, 1996; C.T.M, unpublished observations, Fig. 10). As aptly pointed out by Piotrowski *et al.* (1996), this fact supports the long debated case for serial homology of the cartilages in these arches (e.g., De Beer, 1937; Goodrich, 1930; Kuratani *et al.*, 1997; Schilling and Kimmel, 1997): By this view, morphogenesis in both would be under control by segmentally functioning genes.

The position of the mouth, including the joint between

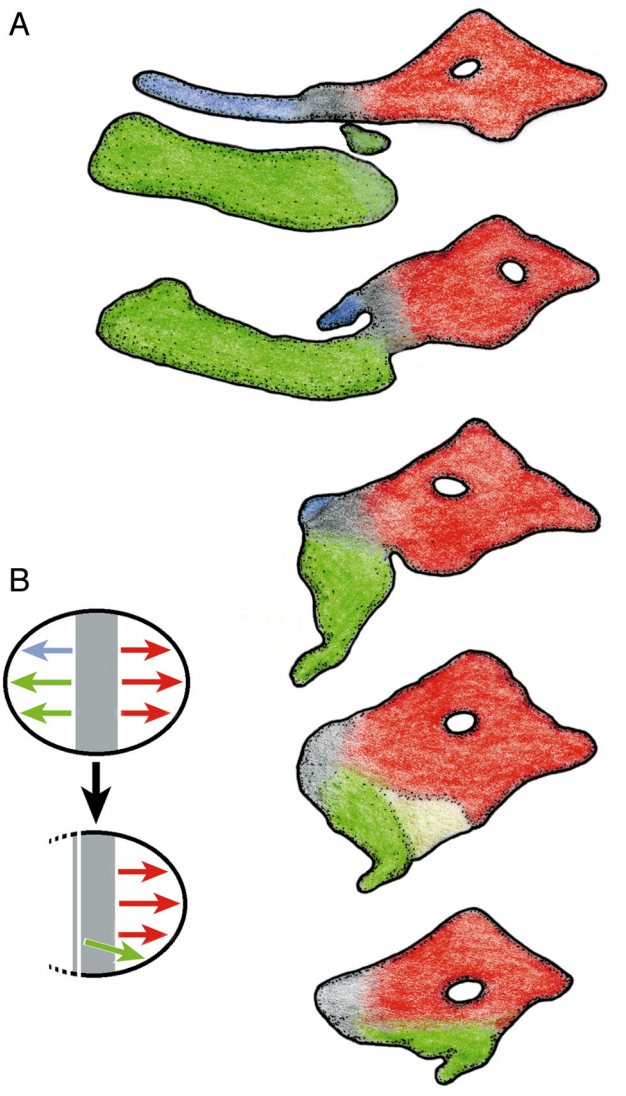

FIG. 11. Ventral defects in cartilage patterning mutants may include a reversal of polarity. (A) An interpretative summary of the phenotypic series in Fig. 9 in which the separate cartilage regions we consider to be present in mutants are given different colors. HM, red; CH and IH, green; SY, blue; IJ, gray. (B) An imaginary scenario of patterning specification in the wild-type precartilage condensation (upper) and the change associated with the most severe mutant phenotype most typical of *suc*$^{-}$ (lower). Note that CH and IH are not distinguished from one another in the model. Within the gray zone (that will develop the IJ and the joint) cells acquire identities indicated by the colors and chondrocyte stack building polarities indicated by the direction of the arrows. Dorsal (red) and ventral (blue, green) polarities are normally opposite, but in the severe mutant cells with ventral identities have dorsal polarities.

the upper and lower jaw, is anterior to the eyes in the zebrafish. This feature differs in fishes deriving from more basal evolutionary lineages, e.g., lampreys, sharks, sturgeons, and the bowfin, *Amia*. In these fish the mouth is ventral and sometimes posterior to the eyes. Hence an anterior mouth would seem to be a derived character in the ray-finned bony fish lineage that includes the teleosts. It is interesting that when the mouth first develops in the zebrafish embryo, it is located ventral and posterior to the eyes, corresponding to what we take to be the primitive position. The mouth then moves anteriorly during the last (third) embryonic day (Schilling and Kimmel, 1997). The relocation involves the anterior elongation (i.e., that we have proposed above is due to the orientation of chondrocyte stack building) of the ventral cartilages in the mandibular and hyoid arches (M and CH). It is this development that fails in *suc*, *she*, and *stu* mutants. Hence the mutations are atavistic in the sense that in mutants the mouth remains in its primitive position (but see Smith and Schneider, 1998, for a cautionary statement concerning interpreting craniofacial mutations as atavisms). Failure of joint formation between the dorsal and ventral mandibular and hyoid cartilages could also be an atavism, since gill arch cartilages in lamprey have no such joint. Whether changes in function of these genes actually figured importantly during gnathostome and teleost evolution seems approachable in comparative studies (Hanken, 1993), providing further motivation to identify the genes molecularly.

Loss of function of any of the genes does not seem to greatly affect the morphogenesis of the HM. This is amazing, considering the severe changes in immediately neighboring cartilages. Possibly another set of genes is required for HM development, genes not uncovered by mutation. The available mutants were picked because of their severe head, mouth, and jaw phenotypes that result secondarily from the cartilage deformations. It is reasonable that specific mispatterning of the dorsal cartilages in these arches might not have the same severe consequences for overall head morphology, at least at early larval stages. New genetic screens, based on Alcian staining in mutagenized larvae to look more directly at cartilage patterning might be a useful way to address this issue.

ACKNOWLEDGMENTS

We thank Tatjana Piotrowski and Christiane Nüsslein-Volhard for providing strains before publication. Tom Schilling and Peter Thorogood critically read drafts of the manuscript. We are grateful to members of the Institute of Neuroscience, University of Oregon, for their interest, insight, and encouragement throughout the course of the study. The research was supported by NIH Grants NS17963 and HD22486. C.T.M. was supported by a NSF predoctoral fellowship, and the work was completed while C.B.K. was a visiting fellow at the Department of Anatomy, University of Cambridge. Support during this sabbatical leave was provided by the Guggenheim Foundation, the NIH Fogarty Senior Fellowship Program, the Anatomical Society of Great Britain and Ireland, and Trinity College. Bill Harris, Roger Keynes, and other members of the Department were particularly generous of their time and resources.

REFERENCES

Beresford, W. A. (1993). Cranial skeletal tissues: Diversity and evolutionary trends. *In* "The Skull" (J. Hanken and B. K. Hall, Eds.). Vol. 2, pp. 69–130.

Bertmar, G. (1959). On the ontogeny of chondral skull in Characidae, with a discussion on the chondroncranial base and the visceral chondrocranium in fishes. *Acta Zool.* **40,** 203–364.

Bryant, P. J. (1996). Cell proliferation control in *Drosophila*: Flies are not worms. *BioEssays* **18,** 781–784.

Clouthier, D. E., Hosoda, K., Richardson, J. A., Williams, S. C., Tanagisawa, H., Kuwaki, T., Kumada, M., Hammer, R. E., and M. Yanagisawa (1998). Cranial and cardiac neural crest defects in endothelin-A receptor-deficient mice. *Development* **125,** 813–824.

Cubbage, C. C., and Mabee, P. M. (1996). Development of the cranium and paired fins in the zebrafish *Danio rerio* (Ostariophysi, Cyprinidae). *J. Morphol.* **229,** 121–160.

Cooper, M. S., D'Amico, L. A., and Henry, C. A. (1997). Analyzing morphogenetic Cell behaviors in living zebrafish embryos. *In* "Protocols in Confocal Microscopy" (S. Paddock, Ed.), "Methods in Molecular Biology" series), Humana Press, Totawa, NJ, in press.

De Beer. G. R. (1937). "The Development of the Vertebrate Skull." Oxford Univ. Press, Oxford, UK. Reprinted 1985, Chicago Univ. Press, Chicago.

Forey, P., and Janvier, P. (1993). Agnathans and the origin of jawed vertebrates. *Nature* **361,** 129–134.

Gendron-Maguire, M., Mallo, M., Zhang, M., and Gridley, T. (1993). *Hoxa-2* mutant mice exhibit homeotic transformation of skeletal elements derived from cranial neural crest. *Cell* **75,** 1317–1331.

Goodrich, E. S. (1930). "Studies on the Structure and Development of Vertebrates." Macmillan, London.

Hall, B. K., and Miyake, T. (1992). The membranous skeleton: The role of cell condensations in vertebrate skeletogenesis. *Anat. Embryol.* **186,** 107–124.

Hanken, J. (1993). Model systems versus outgroups: Alternative approaches to the study of head development and evolution. *Am. Zool.* **33,** 448–456.

Hatta, K., BreMiller, R. A., Westerfield, M., and Kimmel, C. B. (1991). Diversity of expression of *engrailed* homeodomain proteins in zebrafish. *Development* **112,** 821–832.

Honda, H. (1983). Geometrical models for cells in tissues. *In* "International Review of Cytology," Vol. 81, pp. 191–247. Academic Press, New York.

Humphrey, C. D., and Pittman, F. E. (1974). A simple methylene blue–azure II–basic fuchsin stain for epoxy-embedded tissue sections. *Stain Tech.* **42,** 9–14.

Irvine, K. D., and Wieschaus, E. (1994). Cell intercalation during *Drosophila* germband extension and its regulation by pair-rule segmentation genes. *Development* **120,** 827–841.

Kimmel, C. B., Ballard, W. W., Kimmel, S. R., Ullmann, B., and Schilling, T. F. (1995). Stages of embryonic development of the zebrafish. *Dev. Dyn.* **203,** 253–310.

Kimmel, C. B., Warga, R. M., and Kane, D. A. (1994). Cell cycles and clonal strings during formation of the zebrafish central nervous system. *Development* **120,** 265–276.

Kingsley, D. M., Bland, A. E., Grubber, J. M., Marker, P. C., Russell, L. B., Copeland, N. G., and Jenkins, N. A. (1992). The mouse *short ear* skeletal morphogenesis locus is associated with defects in a bone morphogenetic member of the TGF superfamily. *Cell* **71,** 399–410.

Kuratani, S., Matsuo, I., and Aizawa, S. (1997). Developmental patterning and evolution of the mammalian viscerocranium: genetic insights into comparative morphology. *Dev. Dyn.* **209,** 139–155.

Kurihara, Y., Kurihara, H., Suzuki, K., Kodama, T., Maemura, K., Nagai, R., Oda, H., Kuwaki, T., Cao, W. -H., Kamada, N., Jishage, K., Ouchi, Y., Azuma, S., Toyoda, Y., Ishikawa, T., Kumada, M., and Yazaki, Y. (1994). Elevated blood pressure and craniofacial abnormalities in mice deficient in endothelin-1. *Nature* **368,** 703–710.

Milàn, M., Campuzano, S., and García-Bellido (1996). Cell cycling and patterned cell proliferation in the wing primordium of *Drosophila. Proc. Natl. Acad. Sci. U. SA* **93,** 640–645.

Neuhauss, S. C. F., Solnica-Krezel, L., Schier, A. F., Zwartkruis, F., Stemple, D. L., Malicki, J., Abdelilah, S., Stainier, D. Y. R., and Driever, W. (1996). Mutations affecting craniofacial development in zebrafish. *Development* **123,** 357–367.

Newman, S. A., and Comper, W. D. (1990). "Generic" physical mechanisms of morphogenesis and pattern form. *Development* **110,** 1–18.

Piotrowski, T., Schilling, T. F., Brand, M., Jiang, Y.-J., Heisenberg, C. -P., Beuchle, D., Grandel, H., van Eeden, F. J. M., Furutani-Seiki, M., Granato, M., Haffter, P., Hammerschmidt, M., Kane, D. A., Kelsh, R. N., Mullins, M. C., Odenthal, J., Warga, R. M., and Nüsslein-Volhard, C. (1996). Jaw and branchial arch mutants in zebrafish. II. Anterior arches and cartilage differentiation. *Development* **123,** 345–356.

Qiu, M., Bulfone, A., Ghattas, I., Meneses, J. J., Christensen, L., Sharpe, P. T., Presley, R., Pederseon, R. A., and Rubenstein, J. R. (1997). Role of the Dlx homeobox genes in proximodistal patterning of the branchial arches: Mutations of Dlx-1, Dlx-2, and Dlx-1 and -2 alter morphogenesis of the proximal skeletal and soft tissue structures derived from the first and second arches. *Dev. Biol.* **185,** 165–184.

Rijli, F. M., Mark, M., Lakkaraju, S., Dierich, A., Dollé, P., and Chambon, P. (1993). A homeotic transformation is generated in the rostral branchial region of the head by disruption of *Hoxa-2,* which acts as a selector gene. *Cell* **75,** 1333–1349.

Rivera-Perez, J. A., Mallo, M., Gendron-Maguire, M., Gridley, T., and Behringer, R. R. (1995). *goosecoid* is not an essential component of the mouse gastrula organizer but is required for craniofacial and rib development. *Development* **121,** 3005–3012.

Rowe, T. (1996). Coevolution of the mammalian middle ear and neocortex. *Science* **273,** 651–654.

Schilling, T. F. (1997). Genetic analysis of craniofacial development in the vertebrate embryo. *BioEssays* **19,** 459–468.

Schilling, T. F. and Kimmel, C. B. (1994). Segment and cell type lineage restrictions during pharyngeal arch development in the zebrafish embryo. *Development* **120,** 483–494.

Schilling, T. F., and Kimmel, C. B. (1997). Musculoskeletal patterning in the pharyngeal segments of the zebrafish embryo. *Development* **124,** 2945–2960.

Schilling, T. F., Piotrowski, T., Grandel, H., Brand, M., Heisenberg, C. -P., Jiang, Y.-J., Beuchle, D., Hammerschmidt, M., Kane, D. A., Mullins, M. C., van Eeden, F. J. M., Kelsh, R. N., Furutani-Seiki, M., Granato, M., Haffter, P., Odenthal, J., Warga, R. M., Trowe, T., and Nüsslein-Volhard, C. (1996a). Jaw and branchial arch mutants in zebrafish. I. Branchial arches. *Development* **123,** 329–344.

Schilling, T. F., Walker, C., and Kimmel, C. B. (1996b). The *chinless* mutation and neural crest cell interactions in zebrafish jaw development. *Development* **122,** 1417–1426.

Shih, J., and Keller, R. (1992). Cell motility driving mediolateral intercalation in explants of *Xenopus laevis*. *Development* **116,** *901–914*.

Smith, K. K., and Schneider, R. A. (1998). Have gene knockouts caused evolutionary reversals in the mammalian first arch? *BioEssays* **20,** 245–255.

Storm, E. E., Huynh, T. V., Copeland, N. G., Jenkins, N. A., Kingsley, D. M., and Lee, S. -J. (1994). Limb alterations in brachypodism mice due to mutations in a new member of the TGF-β superfamily. *Nature* **368,** 639–643.

Storm, E. E., and Kingsley, D. M. (1996). Joint patterning defects caused by single and double mutations in members of the bone morphogenetic protein (BMP) family. *Development* **122,** 3969–3979.

Subramanian, V., Meyer, B. I., and Gruss, P. (1995). Disruption of the murine homeobox gene *Cdx1* affects axial skeletal identities by altering the mesodermal expression domains of *Hox* genes. *Cell* **83,** 641–653.

Thompson, D. (1942). "On Growth and Form," 2nd. ed. Macmillan, New York.

Thorogood, P. V. (1983). Morphogenesis of cartilage. *In* "Cartilage: Development, Differentiation and Growth" (B. K. Hall, Ed.), Vol. 2, pp. 223–254. Academic Press, New York.

Trelstad, R. L. (1977). Mesenchymal cell polarity and morphogenesis of chick cartilage. *Dev. Biol.* **59,** 153–163.

Weber, R. L., and Blum, H. (1979). Angular invariants in developing human mandibles. *Science* **206,** 689–691.

Westerfield, M. (1995). "The Zebrafish Book." Univ. of Oregon Press.

Wood, A. (1982). Early pectoral fin development and morphogenesis of the apical ectodermal ridge in the killifish, *Aphysemion scheeli*. *Anat. Rec.* **204,** 349–356.

Yamada, G., Mansouri, A., Torres, M., Stuart, E. T., Blum, M., Schultz, M., De Roberts, E. M., and Gruss, P. (1995). Targeted mutation of the murine goosecoid gene results in craniofacial defects and neonatal death. *Development* **121,** 2917–2922.

Yanagisawa, H., Yanagisawa, M., Kapur, R. P., Richardson, J. A., Williams, A. C., Clouthier, D. E., de Wit, D., Emoto, N., and Hammer, R. E. (1998). Dual genetic pathways of endothelin-mediated intercellular signaling revealed by targeted disruption of endothelin converting enzyme-1 gene. *Development* **125,** 825–836.

Received for publication April 21, 1998
Revised July 7, 1998
Accepted July 14, 1998